




OATAO is an open access repository that collects the work of Toulouse researchers and makes it freely available over the web where possible

This is an author's version published in: <http://oatao.univ-toulouse.fr/27990>

Official URL:

<https://doi.org/10.1115/DSCC2019-9184>

To cite this version:

Al Janaideh, Mohammad and Al Saaideh, Mohammad and Rakotondrabe, Micky  *Temperature dependent hysteresis modeling of a piezoelectric tube using Elman neural network.* (2019) In: ASME DSCC Dynamic Systems and Control Conference - DSCC2019, 8 October 2019 - 11 October 2019 (Park City, United States).

Any correspondence concerning this service should be sent to the repository administrator: tech-oatao@listes-diff.inp-toulouse.fr

TEMPERATURE DEPENDENT HYSTERESIS MODELING OF A PIEZOTUBE ACTUATOR USING ELMAN NEURAL NETWORK

Mohammad Al Janaideh

Dept. of Mechanical Engineering
Memorial University
St. John's, NL, Canada *

Mohammad Al Saaideh

Dept. of Electrical Engineering
The University of Jordan
Amman, Jordan

Micky Rakotondrabe

Laboratoire Génie de Production
ENIT, Tarbes, France †

ABSTRACT

In this study, the hysteresis nonlinearities of a piezotube actuator are investigated under different levels of surrounding temperature. The experimental results show that increasing of the surrounding temperature contributes to an increase in the output displacement of the piezotube actuator under the input range that is considered in the experimental tests. In this study, we develop a hysteresis model integrates the dead-zone operator with Elman Neural Network (ENN) to model the temperature-dependent hysteresis nonlinearities. The simulation results show that the proposed temperature-dependent hysteresis model accounts for the temperature effects on the voltage-to-displacement hysteresis nonlinearities. The results show that the proposed model can characterize the voltage-to-displacement hysteresis loops over different levels of surrounding temperature.

1 Introduction

Piezoelectric material-based actuators can perform nanometers resolution displacements at high excitation frequencies with microseconds time constant. Positioning systems driven by piezoelectric material-based actuators have been developed for several micro-and-nano positioning applications and some of them are now commercially available [1–6]. However, these systems show hysteresis nonlinearities that affect the positioning accuracy of these applications. Most of the available studies

on modeling hysteresis of piezoelectric material-based actuators evaluate the hysteresis properties under different input amplitude voltages and frequencies [8–11]. However, these studies ignore the temperature effects on the voltage-to-displacement hysteresis loops. Characterization and modeling of hysteresis nonlinearities under different levels of temperature facilitate the implementation of the piezoelectric material-based actuators in environments that experience steep temperature variations. Such development in hysteresis modeling is mandatory to synthesize an advanced control systems that can reduce the positioning errors over different input voltages and temperature levels.

A number of recent studies have shown that output displacement of a class of piezoelectric material-based actuators is sensitivity to the variation of the surrounding temperature [12, 13]. Such temperature variation can be due to the heating of the surrounding setup (e.g. voltage amplifier) and to the lights that are used to illuminate the tasks [13–15]. However, the effects of the surrounding temperature on the voltage-to-displacement have been ignored. Feedback control systems were designed to reduce the temperature effects under certain conditions in the output of the piezoelectric material-based actuators, see for example [14, 16]. However, it is essential to propose a hysteresis model that considers the temperature effects on the voltage-to-displacement loops. This will develop the model-based control techniques and inverse-based control techniques to compensate for the hysteresis nonlinearities over different temperature levels.

Recently, artificial intelligent algorithms such as Evolution Algorithms, Swarm Algorithms and Neural Network have been widely used for nonlinear systems identification and modeling in science and engineering problems [17–19]. Neural Networks

*Corresponding author, Email: maljanaideh@mun.ca

†Before August 1, 2019, M. Rakotondrabe was with the Department of Automatic Control and Micro-Mechatronic Systems, FEMTO-ST, Université Bourgogne Franche-Comté, CNRS, Besançon France.

have been combined with a number of hysteresis models to characterize the output displacement of a class of smart material-based actuators over different operating conditions. Neural Network with a special operator and transformation was introduced to describe the change tendency of the hysteresis with regard to its input [20,21], hysteretic Recurrent Neural Networks was used to model polycrystalline piezoelectric actuators [22]. Prandtl-Ishlinskii model was combined with neural network to present a hybrid model for hysteresis compensation in piezoelectric actuator [23] and for modeling the hysteresis of magnetostrictive actuator [24]. Beyond neural network modeling, neural network was also used to identify parameters of differential-based and operator-based hysteresis models, see for example [25–29].

An experimental study is first conducted to investigate the effects of the input temperature on the hysteresis nonlinearities of a piezoelectric actuator having tube structure (piezotube). The experimental results are subsequently analyzed to construct an appropriate model that characterizes the hysteresis nonlinearities under different levels of input temperature. This model employs the deadzone operator with the Elman Neural Network (ENN). Then, the proposed model is developed based on the experimental observations. Finally, the model is validated with additional experimental tests. In this study, Section 2 presents a description of an experimental study that was carried out to explore the hysteresis nonlinearities over different levels of environment temperatures. The proposed hysteresis model using the deadzone operator with ENN and the proposed training algorithm are formulated in Section 3. The structure of ENN for proposed hysteresis model and model validations are introduced in Section 4. Finally, the conclusions and future work are presented in Section 5.

2 Experimental Study of Piezotube Actuator

2.1 The Experimental Setup

This section presents a description of the experimental platform that is used to explore the effects of temperature on the voltage-to-displacement hysteresis loops of a piezoelectric actuator. The main objective is to investigate the effects of the temperature levels on the magnitude of the voltage-to-displacement hysteresis loop and the sensitivity of the actuator. The proposed piezoelectric actuator is a piezotube that is classically employed in atomic force microscopy (AFM) [30] and in micro-assembly and micro-manipulation [13]. It is a PT230.94 from PI (Physik Instrumente) company and has 27mm of active length, 5mm of diameter, and 3mm of inner diameter. The actuator can contribute displacements along two horizontal axes (bending along x and y) and along one vertical axis (expansion along z). The output displacement of the actuator in the y -axis is only considered in this study.

A heater resistor, controlled by an electrical current i_T , is used to control the surrounding heat of the actuator and there-

fore to vary its ambient temperature. An optical sensor is placed in front of the extremity of the actuator to measure its bending along the y -axis. The sensor is a LC-2420 from Keyence company with a precision of a hundred nanometers and 10kHz bandwidth. The probe of a thermocouple sensor is integrated inside the heater resistor in order to measure the temperature T assumed to be uniform in the vicinity of the actuator. Finally, a computer with the MATLAB-Simulink software is used to generate all the input signals (u and i_T) and to acquire the measurements temperature T and displacement y . The computer includes an acquisition board dS1103 (from dSPACE) with digital-analog converters (ADC and DAC). Since the generated excitation input signals of the voltage and current from the computer are limited to ± 10 V and to ± 20 mA due to dSPACE requirement, a high-voltage (HV) amplifier of (up to ± 200 V) and a power amplifier of (up to 4 A) are placed between the dSPACE and both the actuator and heater respectively. The data acquisition system sampling time is set to $t_s = 0.2ms$. Figure 1 displays a schematic of the experimental platform that is used to obtain the measured data.

2.2 Temperature-Dependent Hysteresis Characterization

The hysteresis nonlinearities of the piezotube actuator are characterized by applying a harmonic input voltage of $u(t) = 200 \sin(2\pi ft)$ V with excitation frequency $f = 0.1$ Hz at different environment temperatures of $T = 23^\circ C, 29^\circ C, 33^\circ C, 35^\circ C$, and $39^\circ C$. The responses of the actuator to these inputs are illustrated in Figure 2. The figure shows that increasing the environment temperature yields an increase in the global gain (displacement per voltage) of the actuator within the temperature levels considered during the experimental tests. This gain is evaluated using the slope of the best linear model (H) as illustrated in Figure 3 (a). The sensitivity of the actuator are calculated as $0.1509 \mu m/V, 0.1523 \mu m/V, 0.1606 \mu m/V, 0.1627 \mu m/V$, and $0.1735 \mu m/V$ at environment temperatures $T = 23^\circ C, 29^\circ C, 33^\circ C, 35^\circ C$ and $39^\circ C$, respectively. Figure 3 (b) presents the sensitivity as a function of environment temperature that is applied to the actuator. The figure illustrates that increasing the environment temperature contributes an increase in the sensitivity of the actuator within the selected input temperature levels.

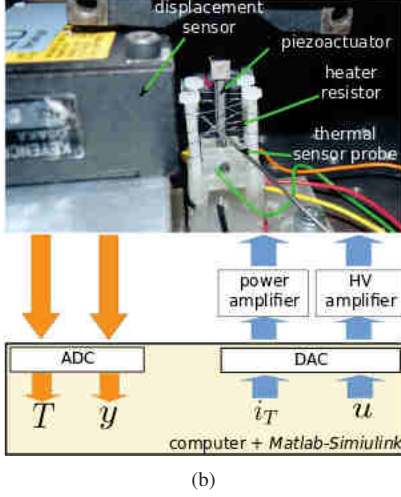
3 Hysteresis Modeling of Piezotube Actuator

3.1 Formulation of the Temperature-Dependent hysteresis model

The proposed Temperature-Dependent hysteresis model for describing the nonlinearities properties of piezotube actuators under the effect of different environment temperatures combines the dead-zone operator with Elman Neural Network (ENN) as the weighting constants. The proposed hysteresis model is illus-



(a)



(b)

FIGURE 1. The experimental platform: (a) PT230.94 piezotube actuator, and (b) PT230.94 piezotube actuator with the displacement sensor, heater resistor, thermal sensor probe, power amplifier, and dSpace card.

trated by the block diagram in Figure 4 (a). For the monotone input $u(t)$ over each sub-interval $[t_{i-1}, t_i]$ defined over the interval $[0, T]$ with N samples and based on the structure of ENN in Figure 4 (b), the output of the proposed hysteresis model at iteration k is formulated as [31]

$$C(k) = H(k-1) + \alpha C(k-1) \quad (1)$$

$$H(k) = f(W_{hi}\Phi(k) + W_{ch}C(k)), \quad (2)$$

$$Y_{est}(k) = g(W_{oh}H(k)), \quad (3)$$

where Φ with size $[n \times N]$ is the output of deadzone operator and represents the input of neural network, C with size $[h \times N]$ is the output of the context layer, H with size $[h \times N]$ is the output of the hidden layer, and Y_{est} with size $[1 \times N]$ is the output of the hysteresis model. The activation functions are $f(x) = 1/(1 + e^x)$ and $g(x) = x$, the connecting weights are W_{hp} , W_{ch} and W_{oh} are weights that are identified through the training algorithm. The output of the deadzone operator for input u and threshold r_m ,

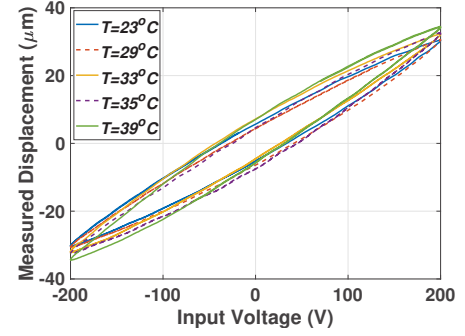


FIGURE 2. Measured voltage-to-displacement hysteresis loops of the piezotube actuator by applying a harmonic input voltage of $u(t) = 200\sin(2\pi ft)$ V with the excitation frequency $f = 0.1$ Hz under different levels of environmental temperature of $T = 23^\circ\text{C}$, 29°C , 33°C , 35°C , and 39°C .

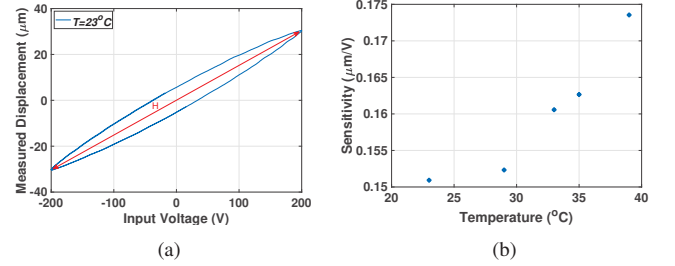


FIGURE 3. (a) The slope of the best linear model of hysteresis loop, and (b) The calculated sensitivity of the piezotube actuator under different levels of environmental temperature of $T = 23^\circ\text{C}$, 29°C , 33°C , 35°C , and 39°C .

where $m = 1, \dots, n$, where n is a positive integer as

$$\Phi_{r_m}[u] = \begin{cases} \max\{u - r_m, 0\} & \text{for } r_m > 0, \\ u & \text{for } r_m = 0, \\ \min\{u - r_m, 0\} & \text{for } r_m < 0, \end{cases} \quad (4)$$

3.2 Training Algorithm

The ENN structure, presented in Figure 4 (b), shows that the neurons in the layers are connected through the weights W_{hp} , W_{ch} and W_{oh} . The sub-indices p indicates the input layer, o indicates the output layer, h indicates the hidden layer, and c indicates the context layer. We define the error between the measured displacement and the output of the hysteresis model as

$$\Sigma[t_i] = \frac{1}{2} (Y_{mes}[t_i] - Y_{est}[t_i])^2, \quad (5)$$

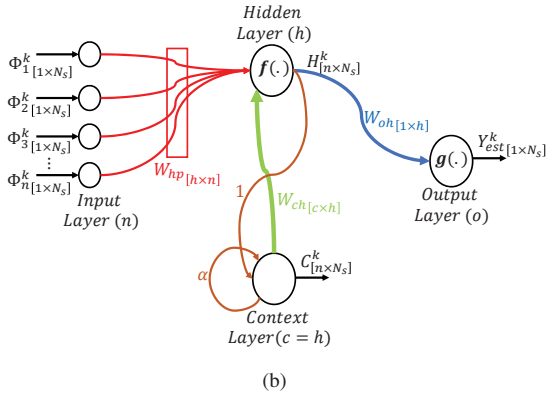
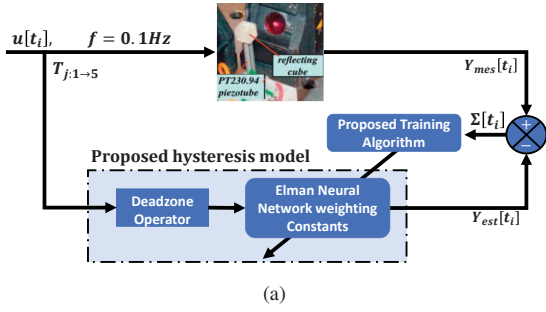


FIGURE 4. (a) Block diagram representation of the proposed hysteresis model, and (b) Feedforward structure of Elman Neural Network (ENN) for the proposed hysteresis model model.

where $Y_{mes}[t_i]$ is the sample of the measured displacement, and $Y_{est}[t_i]$ is the output of the hysteresis model with sample index of $i = 1, 2, \dots, N$. The proposed hysteresis model was obtained by updating the weights W_{hp} , W_{ch} and W_{oh} of ENN to minimize the error in Equation (5) using the Back propagation algorithm [31]. The training algorithm is implemented according as in Figure 5. The following sub-sections present the details.

3.2.1 Dead-zone operator output: In this step, the output of the deadzone operator $\Phi_{rm}[u]$ in Equation (4) is obtained for each input data u_j and using specific threshold number n . The measured data at environment temperatures T_j is presented using j -data sets as Γ_j , where $\Gamma_j = [Y_{mes_j}^T \ \Phi_j^T]$, where Y_{mes_j} is the measured displacement with size $[1 \times N]$ at environment temperature T_j . In this study we consider five tested environment temperatures of $T_j = 23^\circ C, 29^\circ C, 33^\circ C, 35^\circ C,$ and $39^\circ C$, then there it will be five sets of data ($j = 5$).

3.2.2 Data preparing: The data sets Γ_j from the previous step are scaled to be in range of $[0, 1]$. Then, the selected data sets for training process are segmented using specific window size N_s as shown in Figure 6. The segmented data are sep-

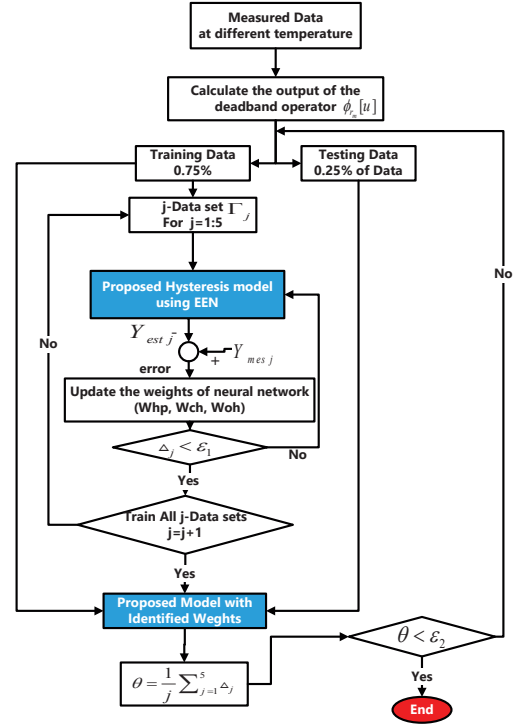


FIGURE 5. Flow chart of training algorithm for proposed hysteresis model.

arated into training data and testing data. The training data with size N_T of 75% of the original samples N are used for training ENN and the testing data of 25% of the original samples N are used for the validation process of ENN. In this study, we use data samples of $N = 750$.

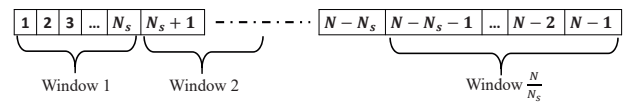


FIGURE 6. Segmentation of data sets using window size N_s .

3.2.3 Elman Neural Network (ENN): This step consists of two algorithms: (i) the feedforward algorithm to obtain the estimated output of proposed hysteresis model, and (ii) the back propagation algorithm to update the weights of ENN. The structure of ENN is determined by selecting the number of neurons in input layer, hidden layer, context layer, and output layer. For the proposed hysteresis model, the number of neurons in the input layer is the threshold number n of dead-

zone operator. In hidden and context layers, the number of neurons can be n or $2n$. The output layer is one neuron. The implementation steps of ENN can be summarized as follows: (i) the values of connecting weights $W_{hp}[h \times n]$, $W_{ch}[h \times h]$, and $W_{oh}[1 \times h]$ are selected randomly then set specific value for learning factor α , (ii) Select the training data set (Γ_j), (iii) apply the Input $\Phi[n \times N_T]$ to the ENN, (iv) obtain the estimated output $Y_{est}[1 \times N_T]$ based on the feedforward algorithm in Equations (1-3), (v) calculate the error between the estimated output and measured output using Equation (5), (vi) apply the back propagation algorithm to update values of connecting weights at the current iteration k based on the following equations $\Delta W_{oh} = \alpha \zeta_o H(k)$, $\Delta W_{hp} = \alpha \zeta_h \Phi(k-1)$, and $\Delta W_{ch} = \alpha \zeta_o W_{oh} \frac{\partial H(k)}{\partial W_{ch}}$, where α is the learning factor, $\zeta_o = (Y_{mes}(k) - Y_{est}(k))g(\cdot)'$, $\zeta_h = (\zeta_o W_{oh})f(\cdot)$ and $\frac{\partial H(k)}{\partial W_{ch}} = f(\cdot)H(k-1) + \beta \frac{\partial H(k-1)}{\partial W_{ch}}$ where $0 < \beta \leq 1$. More details can be found in [31], and (vii) Check if MSE (mean square error) Δ_j of current data sets is less than a specific threshold ε_1 , where $\Delta_j = \frac{1}{N} \sum_{i=1}^N (Y_{mes}[t_i] - Y_{est}[t_i])^2$. If YES go to the next step, If NO go to step (iii) for next iteration. (viii) Check if all j -data sets are trained. If YES go to validation and calculate the MSE of all data sets Θ , If NO go to step (ii) and select the next data set, where the MSE for all data sets is calculated by $\Theta = \frac{1}{j} \sum_{j=1}^5 \Delta_j$.

3.2.4 Testing and Validating Model: In this step, we use the updated weights W_{hp} , W_{ch} , W_{oh} to obtain the estimated output of the proposed hysteresis model and the errors Δ_j and Θ are used to validate the model. If the error Θ is less than specific threshold value ε_2 , the algorithm will be terminated, if not the algorithm will start a new cycle of training.

4 Validation

The measured voltage-to-displacement hysteresis loops illustrated in Figure 2 are used to predict the hysteresis model that is represented using threshold number $n = 9$ for deadzone operators and ENN with the following structure: nine neurons in input layer, five neurons in hidden and context layers, and one neuron in output layer. The learning factor is selected as $\alpha = 0.000975$. Figure 7 presents a comparison between the measured voltage-to-displacement hysteresis loop and the output of the proposed hysteresis model. As the figure illustrates, the proposed hysteresis model can effectively predict the temperature-dependent hysteresis nonlinearities of the piezotube actuator at different levels of temperature.

The characterization errors between the measured output displacement and the proposed hysteresis model output, as shown in Figure 8 (a), are bounded between $[-2\mu m, 2\mu m]$ in the range of $[-30\mu m, 30\mu m]$ displacement. For validations, we obtain the maximum characterization error, the MSE errors, and Roots Mean Square Error (RMSE), where $\Xi_j(t_i) = \sqrt{\Delta_j(t_i)}$. As from Figure 8 (b) the values of MSE and RMS errors are about $1.5\mu m$

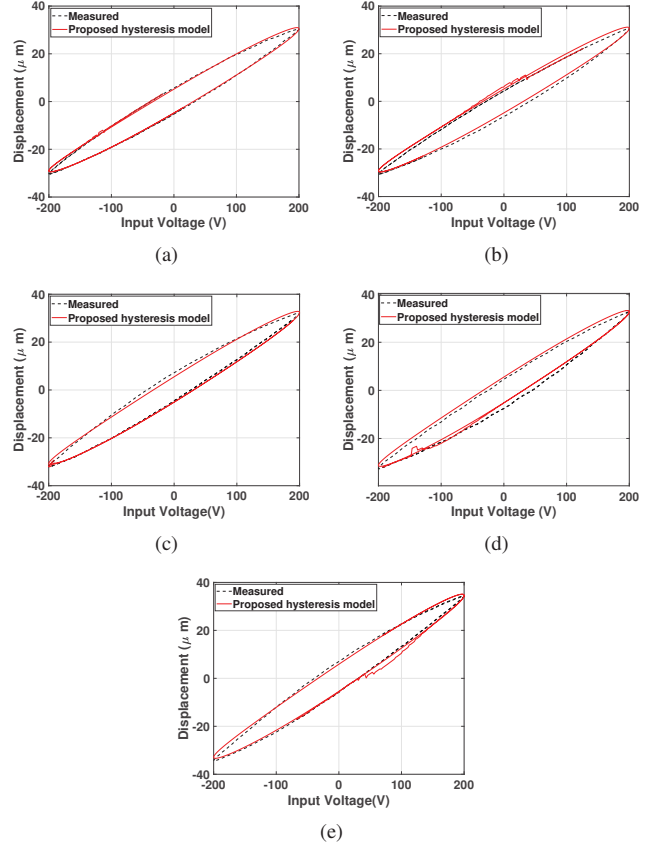


FIGURE 7. Comparison between the measured voltage-displacement hysteresis loop and the proposed hysteresis model voltage-displacement hysteresis loop using threshold number of $n = 9$ at different environmental temperatures: (a) $T = 23^\circ C$, (b) $T = 29^\circ C$, (c) $T = 33^\circ C$, (d) $T = 35^\circ C$, and (e) $T = 39^\circ C$.

and the maximum error is between $2\mu m$ and $3\mu m$. In addition, the proposed hysteresis model shows similar sensitivity to the experimental observation. The model shows that the sensitivity increases when the environmental temperature increases, as shown in Figure 8 (c).

Also, the hysteresis model is obtained using threshold number $n = 5$ for the deadzone operator and ENN with five neurons in the input layer, ten neurons in hidden and context layers, and one neuron in the output layer. In this case, the learning factor is $\alpha = 0.001$. The resulting error is illustrated in Figure 9. By comparing the results in Figure 8 and the results in Figure 9, we conclude that hysteresis model with $n = 9$ gives better characterization in comparison with $n = 5$. During the training process of the ENN, it was observed that selecting values of learning factor α and selecting number of neurons in ENN have an important role for the algorithm convergence and obtaining better modeling results.

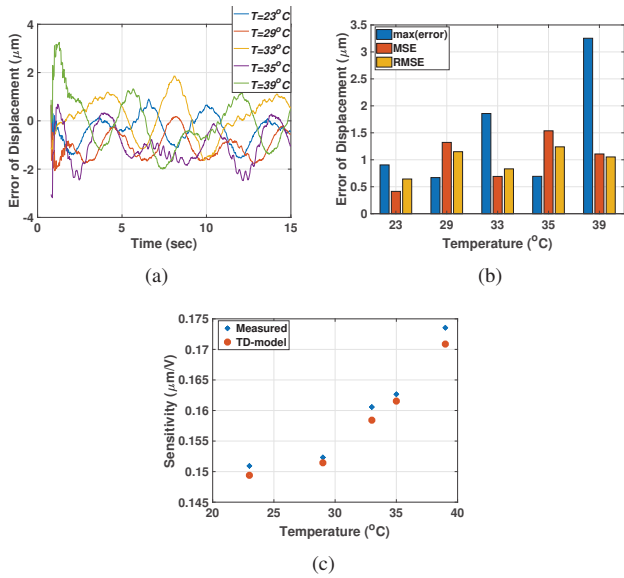


FIGURE 8. (a) Error signal between the measured output displacement and the proposed hysteresis model output using threshold number $n = 9$ at different environmental temperatures, (b) Maximum error, Mean square error (MSE) and Root mean square error (RMSE) for the measured output displacement and the proposed model hysteresis output, and (c) comparison of the sensitivity of the measured data and the proposed hysteresis model.

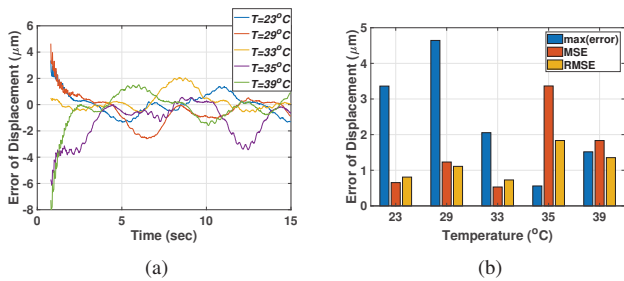


FIGURE 9. (a) Error signal between the measured output displacement and the proposed hysteresis model output using threshold number $n = 5$ at different environmental temperatures, and (b) Maximum error, Mean square error (MSE) and Root mean square error (RMSE) for the measured output displacement and the proposed hysteresis output,

5 Conclusions

The output displacement of a piezotube actuator was characterized under different levels of environmental input temperature. The results demonstrate that increasing the temperature

contributes an increase in the sensitivity of the actuator within the operating range that was considered in the experimental study. The proposed hysteresis model that integrates the dead-zone operator with Elman Neural Network was formulated using the experimental observations. The proposed hysteresis model was able to describe the hysteresis nonlinearities under different levels of temperatures that were imposed to the piezotube actuator. The estimated output of the proposed hysteresis model and the calculations of error show the validity of using this model to describe the hysteresis nonlinearities of piezotube actuator under different levels of environmental temperatures.

The results of this study can be extended in the future work to include modeling and experimental compensation of temperature-dependent hysteresis properties of the actuator in both horizontal and vertical axes. In addition to that, the proposed Neural Network hysteresis model can be modified to obtain the inverse of the hysteresis model for compensation of hysteresis nonlinearities in an open-loop and closed-loop manners.

6 Acknowledgments

This work has been supported by 2018 Mobility Funding for France-Canada Researchers (Embassy of France in Ottawa) and the EIPHI Graduate school (contract "ANR-17-EURE-0002").

REFERENCES

- [1] Smith, R., *Smart material systems: model development*, Society for Industrial and Applied Mathematics, 2005.
- [2] Crews, J., Bravo, N. and Smith, R., "Model development for PZT bimorph actuation employed for micro-air vehicles," *Proceedings of ASME Conference on Smart Materials, Adaptive Structures and Intelligent Systems*, pp. 1-6, 2016.
- [3] Farrokh, M. and Dizaji, M., "Adaptive simulation of hysteresis using neuro-Madlung model," *Journal of Intelligent Material Systems and Structures*, vol. 27, pp. 1713-1724, 2016.
- [4] Liang, S., Boudaoud, M., Cagneau, B. and Regnier, S., "Velocity characterization and control strategies for nanorobotic systems based on piezoelectric stick-slip actuators," *Proceedings of IEEE International Conference on Robotics and Automation*, pp. 6606-6611, 2017.
- [5] Xiong, R., Liu, X. and Lai, Z., "Heuristic modeling and inverse compensation of hysteresis in piezoelectric actuators based on time series similarity," *Journal of Intelligent Material Systems and Structures*, vol. 27, pp. 1814-1828, 2016
- [6] Stefanski, F., Minorowicz, B., Persson, J., Plummer, A. and Bowen, C., "Non-linear control of a hydraulic piezo-valve using a generalised Prandtl-Ishlinskii hysteresis model," *Mechanical Systems and Signal Processing*, vol. 82, pp. 412-431, 2017.

- [7] Zakerzadeh, M. and Sayyaadi, H., "Precise position control of shape memory alloy actuator using inverse hysteresis model and model reference adaptive control system," *Mechatronics*, vol. 23, pp. 1150-1162, 2013.
- [8] Rakotondrabe, M., "Multivariable classical Prandtl-Ishlinskii hysteresis modeling and compensation and sensorless control of a nonlinear 2-dof piezoactuator," *Nonlinear Dynamics*, vol. 89, pp. 481-499, 2017.
- [9] Davino, D., Krejci, P. and Visone, C., "Fully coupled modeling of magneto-mechanical hysteresis through thermodynamic compatibility," *Smart Materials and Structures*, vol. 22, pp. 1-14, 2013.
- [10] Al Janaideh, M., Rakotondrabe, M. and Aljanaideh, O., "Further results on hysteresis compensation of smart micro-positioning systems with the inverse Prandtl-Ishlinskii compensator," *IEEE Transactions on Control Systems Technology*, vol. 24, pp. 428-439, 2016.
- [11] Aljanaideh, O., Al Janaideh, M. and Rakotondrabe, M., "Enhancement of micro-positioning accuracy of a piezoelectric positioner by suppressing the rate-dependant hysteresis nonlinearities," *Proceedings of IEEE/ASME International Conference on Advanced Intelligent Mechatronics*, pp. 1683-1688, 2014.
- [12] Khler, R. and Rinderknecht, S., "A phenomenological approach to temperature dependent piezo stack actuator modeling," *Sensors and Actuators A: Physical*, vol. 200, pp. 123-132, 2013.
- [13] Habineza, D., Zouari, M., Hammouche, M., Le Gorrec, Y. and Rakotondrabe, M., "Characterization and modeling of the temperature effect on the piezoelectric tube actuator," *IFAC-PapersOnLine*, vol. 49, pp. 354-360, 2016.
- [14] Hammouche, M., Lutz, P., and Rakotondrabe, M., "Robust and guaranteed output-feedback force control of piezoelectric actuator under temperature variation and input constraints," *Asian Journal of Control*, 2019.
- [15] Ganley, T., Hung, D., Zhu, G. and Tan, X., "Modeling and inverse compensation of temperature-dependent ionic polymer-metal composite sensor dynamics," *IEEE/ASME Transactions on Mechatronics*, vol. 16, pp. 80-89, 2010.
- [16] Rakotondrabe, M., Diouf, M. and Lutz, P., "Robust feedforward-feedback control of a hysteretic piezocantilever under thermal disturbance," *IFAC Proceedings Volumes*, vol. 41, pp. 13725-13730, 2008.
- [17] Nguyen, S., HoHuu, V. and Ho, A., "A neural differential evolution identification approach to nonlinear systems and modelling of shape memory alloy actuator", *Asian Journal of Control*, vol. 20, pp.57-70, 2018.
- [18] Cuevas, E., Daz, P., Avalos, O., Zaldvar, D. and Prez-Cisneros, M., "Nonlinear system identification based on ANFIS-Hammerstein model using Gravitational search algorithm," *Applied Intelligence*, vol. 48, pp. 182-203, 2018.
- [19] Anh, H., Son, N., Van Kien, C. and Ho-Huu, V., "Parameter identification using adaptive differential evolution algorithm applied to robust control of uncertain nonlinear systems," *Applied Soft Computing*, vol. 71, pp. 672-684, 2018.
- [20] Ayala, H., Habineza, D., Rakotondrabe, M., Klein, C. and Coelho, L., "Nonlinear black-box system identification through neural networks of a hysteretic piezoelectric robotic micromanipulator," *IFAC-PapersOnLine*, vol. 48, pp. 409-414, 2015.
- [21] Zhang, X., Tan, Y. and Su, M., "Modeling of hysteresis in piezoelectric actuators using neural networks," *Mechanical Systems and Signal Processing*, vol. 23, pp. 2699-2711, 2009.
- [22] Lien, J., York, A., Fang, T. and Buckner, G., "Modeling piezoelectric actuators with hysteretic recurrent neural networks," *Sensors and Actuators A: Physical*, vol. 163, pp. 516-525, 2010.
- [23] Chen, Y., Qiu, J. and Sun, H., "A hybrid model of Prandtl-Ishlinskii operator and neural network for hysteresis compensation in piezoelectric actuators," *International Journal of Applied Electromagnetics and Mechanics*, vol. 41, pp. 335-347, 2013.
- [24] Wang, Y., Xu, R. and Zhou, M., "Prandtl-Ishlinskii modeling for giant magnetostrictive actuator based on internal time-delay recurrent neural network," *IEEE Transactions on Magnetics*, vol. 54, pp. 1-4, 2018.
- [25] Wang, G. and Chen, G., "Identification of piezoelectric hysteresis by a novel Duhem model based neural network," *Sensors and Actuators A: Physical*, vol. 264, pp. 282-288, 2017.
- [26] Xu, R. and Zhou, M., "Elman neural network-based identification of Krasnoselskii-Pokrovskii model for magnetic shape memory alloys actuator," *IEEE Transactions on magnetics*, vol. 53, pp. 1-4, 2017.
- [27] Zhang, X., Tan, Y., Su, M. and Xie, Y., "Neural networks based identification and compensation of rate-dependent hysteresis in piezoelectric actuators," *Physica B: Condensed Matter*, vol. 405, pp. 2687-2693, 2010.
- [28] Wang, X. and Li, G., "Rate-dependent hysteresis modeling for fast tool servo system based on RBF neural networks," *Proceedings of the International Conference on Mechatronics and Automation Engineering*, pp. 295-302, 2017.
- [29] Fan, Y. and Tan, U., August, "Adaptive rate-dependent feedforward control for piezoelectric actuator," *Proceeding of 13th IEEE Conference on Automation Science and Engineering*, pp. 592-597, 2017.
- [30] Binnig, G., Quate, C. and Gerber, C., "Atomic force microscope," *Physical review letters*, vol. 56, pp. 930-933, 1986.
- [31] Hongmei, L., Shaoping, W. and Pingchao, O., "Fault diagnosis based on improved Elman neural network for a hydraulic servo system," *Proceedings of IEEE Conference on Robotics, Automation and Mechatronics*, pp. 1-6, 2016.